Steady-state deformation behavior of confined composite droplets under shear flow

Stanislav Patlazhan,[1,*] Sergei Vagner,[2] and Igor Kravchenko[2]

[1]*Semenov Institute of Chemical Physics of Russian Academy of Sciences, 4, Kosygin Street, Moscow, 119991, Russia*

[2]*Institute of Problems of Chemical Physics of Russian Academy of Sciences, 1, Semenov Avenue, Chernogolovka, Moscow Region, 142432, Russia*

(Received 22 February 2015; published 4 June 2015)

The shear-induced dynamics of two-dimensional composite droplets in a narrow channel is investigated numerically. The droplets consist of a viscous inner droplet (core) and shell immersed in a continuous Newtonian fluid. Attention is focused on studying the effects of confinement at different core-to-shell radii ratios, relative viscosities of the medium components, and interfacial tensions on the steady-state deformation and orientation of a composite droplet. The role of the "sustaining" effect due to the internal core and competition between the near-wall shear flow and downward and upward secondary streams is discussed.

DOI: 10.1103/PhysRevE.91.063002 PACS number(s): 47.61.−k, 47.57.−s

I. INTRODUCTION

The hydrodynamics of multiphase fluids is of significant scientific and practical interest in relation to the problems of processing incompatible polymer blends, the transportation of petroleum products, the development of new composite materials, and applications in food and cosmetic industries, as well as medical and biological uses. One of the key problems is the deformability and ultimate properties of dispersed phase in different flow conditions. The attention was mainly focused on studying the dynamic behavior of homogeneous droplets [1–4]. The obtained body of knowledge provides the modern understanding of the dynamic processes occurring in dispersion media. On the other hand, the advancement in modern materials calls for the investigation of more complex problems, including the hydrodynamic behavior of heterogeneous (composite) drops. Such problems arise in the analysis of the structure and dynamic behavior of ternary polymer blends [5–8], double emulsions, capsules and vesicles [9–14], encapsulation of food ingredients, drug delivery [15–17], and so on. In the simplest case, the composite drops consist of a viscous core surrounded by a liquid shell. The formation of such droplets through the engulfing of one dispersed phase by another along with their deformation behavior under shear flow were studied experimentally by Torza and Mason [9]. In contrast to homogeneous droplets, the hydrodynamic behavior of composite droplets is determined by multiple parameters: viscosity ratios of the components, core-to-shell radii ratio, and core-shell and shell-continuum phase interfacial tensions. This greatly complicates the problem solution.

Among the early theoretical works, the study of the hydrodynamic behavior of composite drops at low Reynolds and capillary numbers should be mentioned. The drag force and change in shape of concentric spherical composite droplets under axisymmetric creeping flow [18–20] along with the hydrodynamic behavior of eccentric composite viscous core-shell droplets [21] were studied. This problem has also been considered with regard to a solid core (ice particle) [22]. The obtained solutions are limited to small deformations. Generally they are not applicable for predicting large deformations and break-up of droplets. This point was emphasized by Stone and Leal [23], who found analytical solutions for weakly deformed and numerical results for strongly deformed composite droplets at both uniaxial and biaxial drag flows. Their analysis showed that the deformation behavior of the composite droplets may vary significantly with a change of flow type. For instance, recirculation of fluid in the outer layer arising with axisymmetric flow results in drop flattening and the extension of its core along the flow direction, whereas the opposite situation takes place under biaxial extensional flow. It was noted that the core viscosity has little influence on the overall deformation of the droplets. This result was taken into account in modeling of leukocyte dynamics [24].

The hydrodynamic behavior of composite droplets under shear flow has mainly been studied by means of computer simulation. Among the theoretical works on this topic, we managed to find only a purely mathematical paper [25] arguing that integral representation of the Stokes equations for a medium containing a composite droplet has a unique solution for the velocity field at arbitrary viscosity ratios. The dynamic behavior and break-up of composite droplets in shear flow was first investigated numerically in the example of equiviscous components [26] by means of the level set function method [27]. It was shown that variation in interfacial tensions could lead to new peculiarities in the deformation of the droplets as well as break-up of their nuclei. On the other hand, it was found that shear flow could alter significantly the internal structure of two-dimensional (2D) composite droplets with a low-viscous core [28]. This paper also demonstrated that shear flow promotes the ousting of a core from a viscous envelope if the core-to-shell interfacial tension is large enough (the so-called "washing" effect). The systematic numerical simulation of shear-induced steady-state deformation and break-up of the unbounded viscous composite droplets at different capillary numbers, viscosity, and radii ratios were reported in Ref. [29]. It was shown that equiviscous composite droplets are deformed due to the vortex flow located within the shell. In this case, as in the axisymmetric flow, the core viscosity has little effect on the overall deformation of the composite droplets. By contrast, variation of shell viscosity has a significant impact on deformation and spatial orientation of the droplets. Numerical simulation of 2D composite droplets

*sapat@yandex.ru

with a high-viscosity core and low-viscosity shell showed [30] that at low values of capillary and Reynolds numbers and reasonably high core-shell interfacial tension, the steady-state form of the outer layer resembles the shape of the water layer released from a hydrogel under shear flow [31]. In contrast to the homogeneous drops, the major axis of the considered composite droplets is aligned with the flow direction.

In recent years, a significant interest in the hydrodynamic behavior of droplets confined in narrow channels has been manifested. This is primarily prescribed by the problems of microfluidics using the flow of multiphase fluids in channels with transverse dimensions of the order of several tens of microns [32–34]. Solving such problems is of fundamental importance in understanding emulsion flow under the confinement conditions and engineering of microfluidic devices. Meanwhile, experimental studies have established a number of unusual effects associated with the two-phase fluid flow in the narrow channels. In particular, droplet-string transitions were found in the dispersion of polydimethylsiloxan in a polyisobutylene matrix with close viscosities when the size of minor phase domains became comparable to the distance between the shearing walls [35,36]. It was shown that confinement favors an increase in droplet elongation and suppresses the development of Rayleigh capillary instability. This finding was confirmed by Sibillo *et al.* [37], showing also that a decrease of the channel thickness leads to a decrease in the orientation angle of a homogeneous droplet with respect to flow direction. These conclusions were extended to various droplet-to-matrix viscosity ratios [38]. In particular, it was emphasized that unlike the above-described system, confinement favors disintegration of a droplet if its viscosity exceeds the viscosity of the continuous media.

The theory of deformation of a homogeneous droplet in the Stokes shear flow between two parallel walls has been developed using the Lorentz reflection method [39]. The obtained correction to the well-known Taylor formula [40] provided the additional strain caused by the influence of the channel walls, which is proportional to the cube of the confinement parameter $n = (2a/h)^3$, where a and h are the droplet radius and channel thickness, respectively. The resulting solutions coincide with the experimental data for the droplets in the equiviscous fluid [37], but they do not correspond to measurements at large viscosity ratio. This inconsistence was overcome with the help of a phenomenological approach [41] based on the modified theory [42] assuming an ellipsoidal droplet shape. Numerical simulation of the deformation behavior of a droplet confined between parallel rigid walls showed [42,44] that the increase of its deformation in comparison with the unbounded droplets is caused by the pronounced increase in the shear rate between the droplet ends and moving walls. These outcomes were confirmed by lattice-Boltzmann simulations [45].

The interest in the study of the dynamic behavior of composite droplets in narrow channels is defined by issues related to the passage of red blood cells and leucocytes in blood vessels [46,47] as well as the production of functional pharmaceutical compositions by means of microfluidic technologies [48–51]. At the same time, these effects have not received systematic investigation. In this work we do not consider the ultimate properties of the droplets and restrict our study to the steady-state deformation behavior of 2D composite droplets subjected to a simple shear flow in a narrow channel by means of numerical simulations. Attention will be focused on revealing the dependences of deformation and orientation angle of a composite droplet on the (1) confinement parameter, (2) core-to-shell radii ratio, (3) viscosity ratios, (4) ratios of the interfacial tensions, and (5) capillary number. The dynamic behaviors of the unbounded and confined composite droplets will be compared.

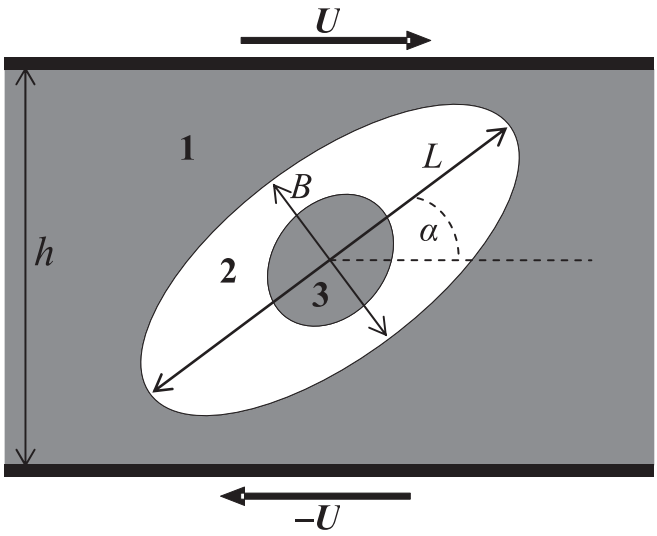

FIG. 1. Computational domain containing the deformed composite droplet.

II. NUMERICAL SIMULATION

A. Model

We consider the shear flow of an incompressible medium containing a 2D concentric composite droplet placed between parallel rigid walls moving in opposite directions with equal rates U (see Fig. 1). To avoid translational motion, the droplet is placed at the center of the computational domain. The periodic boundary conditions of fluid velocity and pressure are imposed on the side faces of the cell. They are placed far apart from the droplet to minimize the flow perturbations.

The distance between the walls (channel thickness) is h, while the initial radii of the shell and core of the composite droplet are denoted as a and b, respectively. The gap between the walls is filled by the continuous phase 1 of viscosity μ_1; the viscosities of liquid shell 2 and core 3 of the composite droplet are equal to μ_2 and μ_3, respectively, while the densities of all components are assumed to be equal to each other, $\rho_1 = \rho_2 = \rho_3$. The interfacial tensions on the external and internal boundaries of the composite droplet are equal to σ_{12} and σ_{23}, respectively. The simulation results will be expressed in terms of dimensionless parameters as $n = 2a/h$ confinement parameter, $k = b/a$ radii ratio, $m_{i1} = \mu_i/\mu_1$ viscosity ratio of the ith component to the continuous phase, and $\kappa = \sigma_{23}/\sigma_{12}$ ratio of the interfacial tensions. The overall stretching of a droplet was estimated in terms of the Taylor deformation parameter $D = (L - B)/(L + B)$ [40], where L and B are the maximum and minimum distances from the center of the drop to its outer boundary (see Fig. 1). The orientation angle

α of the droplet is defined as the inclination of the elongation axis with respect to the flow direction.

The velocity distribution $\boldsymbol{u}_i(\mathbf{x},t)$ in the ith component of the three-component system under consideration is governed by the Navier-Stokes equations

$$\rho_i\left(\frac{\partial \boldsymbol{u}_i}{\partial t}+(\boldsymbol{u}_i\cdot\nabla)\boldsymbol{u}_i\right) = -\nabla p_i+\nabla[\mu_i(\nabla\boldsymbol{u}_i+(\nabla\boldsymbol{u}_i)^T)]+\mathbf{F}_{ij}\quad(i,j=1,2,3) \tag{1}$$

and the incompressibility conditions

$$\nabla\cdot\boldsymbol{u}_i=0\quad(i=1,2,3). \tag{2}$$

The volume force $\mathbf{F}_{ij}$ in Eq. (1) corresponds to the Laplace capillary force localized on one of the interfaces S_{12} and S_{23} of the composite droplet. It can be represented as [52]

$$\mathbf{F}_{ij}(\mathbf{x})=-\sigma_{ij}\zeta_{ij}(\mathbf{x}_{S_{ij}})\boldsymbol{n}_{ij}(\mathbf{x}_{S_{ij}})\delta(\mathbf{x}-\mathbf{x}_{S_{ij}})\quad i\neq j, \tag{3}$$

where $\delta(\mathbf{x}-\mathbf{x}_{S_{ij}})$ is the Dirac delta function with support on the interface S_{ij} between components i and j; ζ_{ij} and $\boldsymbol{n}_{ij}$ are the curvature and unit normal at the point $\mathbf{x}_{S_{ij}}$ of the interface. Actually, integration of $\mathbf{F}_{ij}(\mathbf{x})$ over the small volume including a small portion of the interface gives the surface force $-\sigma_{ij}\zeta_{ij}(\mathbf{x}_{S_{ij}})\boldsymbol{n}_{ij}(\mathbf{x}_{S_{ij}})dS_{ij}$ applied at the point $\mathbf{x}_{S_{ij}}$.

B. Modeling of interface dynamics

To calculate the current position of the interfaces of the liquid composite droplet, the level set method was applied [27,53]. In this approach, position $\mathbf{x}$ of any interfacial point is defined by the coordinates of the zero level of a smooth function $\phi(\mathbf{x},t)$. This function represents a distance from the nearest boundary S_{ij}, so that $\phi(\mathbf{x},t)$ possesses opposite signs in the conjugate phases. The disadvantage of this method is attributable to the possible volume loss when a dispersed phase is commensurate with a few cells of a computational grid. In this paper we do not consider the droplet break-up into smaller parts so that the loss of its volume is negligible.

Since the interfacial boundaries of a composite droplet are changed during shear flow, their positions at each instant of time are described by the continuity equation of the level set function

$$\frac{\partial\phi}{\partial t}+\boldsymbol{u}\cdot\nabla\phi=0, \tag{4}$$

where $\boldsymbol{u}$ is the local flow velocity. Knowing $\phi(\mathbf{x},t)$ we can define the unit normal vector and curvature at any point of an interface: $\mathbf{n}=(\nabla\phi/|\nabla\phi|)|_{\phi=0}$ and $\zeta=\nabla\cdot(\nabla\phi/|\nabla\phi|)|_{\phi=0}$. To smooth out the viscosity jumping on passage from one phase to another, a symmetric transition layer of 2ε width is introduced. Then the local viscosity ratio of the three-phase system with equiviscous core and continuous phase can be represented as a continuous function $\mu(\phi)=m_{21}+(1-m_{21})H(\phi)$, where $H(\phi)$ is the smoothed Heaviside function, which is equal to $H(\phi)=0$ if $\phi<-\varepsilon$, $H(\phi)=0.5[1+\phi\varepsilon^{-1}+\pi^{-1}\sin(\pi\phi\varepsilon^{-1})]$ if $|\phi|\leqslant\varepsilon$, and $H(\phi)=1$ if $\phi>\varepsilon$. The width of the transition layer is typically chosen to be equal to several grid cells. This approximation allows us to eliminate singularities in the spatial derivatives of viscosity.

TABLE I. Steady-state deformation and orientation angle versus mesh size and time step.

n	Number of cells	Mesh size, Δx	Time step, Δt	D	α, deg.
1	512 × 128	$3.9\,10^{-2}$	10^{-3}	0.235	29.845
2	512 × 128	$3.9\,10^{-2}$	10^{-4}	0.2238	26.939
3	1024 × 256	$1.9\,10^{-2}$	10^{-4}	0.2244	27.121
4	1024 × 256	$1.9\,10^{-2}$	10^{-5}	0.2223	26.939

In such a manner the three-phase system can be considered as a single medium with material characteristics depending on the level set function ϕ. The capillary forces in turn are approximated by volume forces concentrated in a narrow transition layer. Introducing a unit of length as the external radius a of the composite droplet, a unit velocity as the wall rate U, and viscosity and density units as being equal to viscosity and density μ_1 and ρ_1 of the continuous phase 1, respectively, the Navier-Stokes equations (1) and the incompressibility conditions (2) can be represented in the following dimensionless equations [53]:

$$\frac{\partial\boldsymbol{u}}{\partial t}+(\boldsymbol{u}\cdot\nabla)\boldsymbol{u}=-\nabla p+\frac{1}{\mathrm{Re}}\left\{\nabla\cdot[\mu(\phi)(\nabla\boldsymbol{u}+(\nabla\boldsymbol{u})^T)]-\frac{1}{\mathrm{Ca}(\phi)}\zeta(\phi)\delta(\phi)\nabla\phi\right\}, \tag{5}$$

$$\nabla\cdot\boldsymbol{u}=0, \tag{6}$$

where capillary number $\mathrm{Ca}(\phi)$ is equal to $\mathrm{Ca}=\mu_1 U a\sigma_{12}^{-1}$ if point $\mathbf{x}$ is located at the smeared interface S_{12} or $\mathrm{Ca}\sigma_{12}\sigma_{23}^{-1}$ if $\mathbf{x}$ belongs to the interface S_{23}; $\mathrm{Re}=Ua\rho_1\mu_1^{-1}$ is the Reynolds number. The smoothed Dirac delta function is defined as $\delta(\phi)=\frac{dH(\phi)}{d\phi}=\frac{1}{2\varepsilon}[1+\cos(\pi\phi/\varepsilon)]$ if $|\phi|\leqslant\varepsilon$ or $\delta(\phi)=0$ if $|\phi|>\varepsilon$.

For the numerical solution of Eqs. (4)–(6), the projection method was employed [54]. According to this method, Eq. (5) is divided into three simpler equations. In the first stage, the intermediate velocity field $\boldsymbol{u}^*$ is calculated with zero pressure gradient. Then the pressure p is calculated from the Poisson equation, the right-hand side of which includes divergence of the intermediate velocity. Based on the resulting solutions and the incompressibility condition (6), the velocity correction is carried out at the next time step. To eliminate errors arising in the numerical solution of Eq. (4), the periodic recovery procedure [27] for the level set function $\phi(\mathbf{x},t)$ is applied.

To optimize the accuracy of numerical estimation of these characteristics, the influence of the mesh size Δx and time step Δt was analyzed (see Table I). To this end, a series of runs was performed on a square mesh of various density and different time steps with the example of the homogeneous droplet at $\mathrm{Ca}=0.2$, $\mathrm{Re}=0.1$, $m_{21}=0.1$, $n=0.4$. It can be seen that with decreasing time steps and mesh size, convergence of the obtained solutions to the fixed values of steady-state deformation D and orientation angle α is observed. From the data obtained it follows that a 512 × 128 grid and the time step $\Delta t=10^{-4}$ are appropriate for use, as a further reduction of the steps in space and time would lead to minor changes in these characteristics.

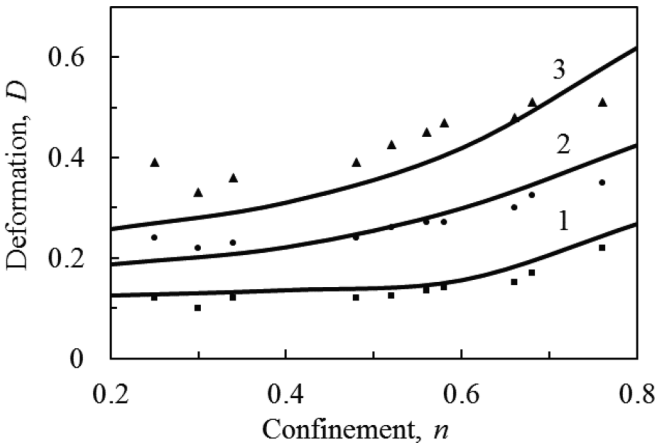

FIG. 2. Steady-state deformation of homogeneous droplet in shear flow vs confinement parameter n for equiviscous system at $\mathrm{Re} = 0.05$, and different capillary numbers $\mathrm{Ca} =$ (1) 0.1 (2) 0.2 (3) 0.3. The solid lines correspond to the 2D droplet; the symbols represent experimental data [37].

C. Comparative modeling

Before proceeding to discuss the hydrodynamics of a composite droplet in a narrow channel, we should compare some of our solutions with some known numerical and experimental results [29,37]. Figure 2, in particular, shows the stationary deformation of the homogeneous droplet in the equiviscous continuous medium under simple shear flow as a function of confinement parameter n at Reynolds number $\mathrm{Re} = 0.05$ and different capillary numbers $\mathrm{Ca} = 0.1, 0.2, 0.3$. Symbols denote the experimental data [37] while solid lines correspond to our results for the 2D droplet. It is evident that the experimental and numerical results for three-dimensional (3D) and 2D droplets are qualitatively consistent with each other. They show that in both cases the droplet distension grows with the confinement and capillary number, with the deformation of the 2D droplet achieving almost complete agreement with the experiment at $\mathrm{Ca} = 0.1$.

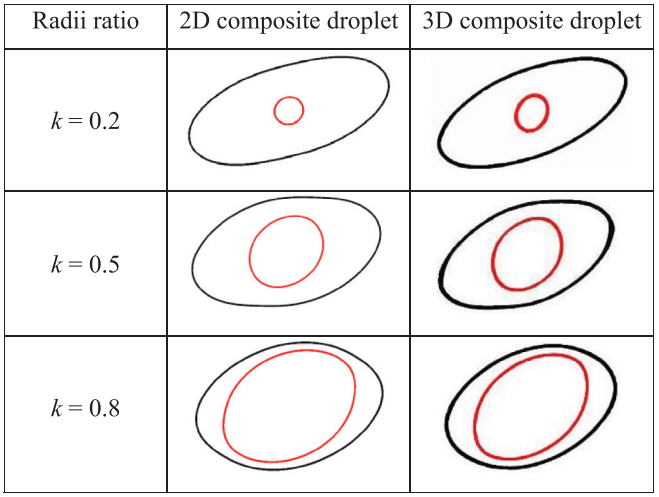

FIG. 3. (Color online) Steady-state shapes of the unbounded 2D (our calculations) and 3D [29] composite droplets at different radii ratios k at $\mathrm{Ca} = 0.4$, $m_{21} = m_{31} = 1$, $\kappa = 1$.

Figure 3 shows the shear-induced steady-state shapes of the unbounded 2D and 3D composite equiviscous droplets calculated at $\mathrm{Re} = 0.05$ and $\mathrm{Ca} = 0.4$ for different values of radii ratio k. Two-dimensional droplets represent our simulations by level set function method, while 3D droplets were modeled using a volume of fluids method. It is evident that the shapes of 2D and 3D drop models are in qualitative agreement.

The above examples allow one to conclude that our calculations are in good agreement with known experimental and numerical results, which proves the adequacy of the approach used in this paper.

III. RESULTS AND DISCUSSION

A. The effect of confinement

Along with the homogeneous droplet [37,43], confinement has a significant impact on the deformation behavior of the composite droplet. This is demonstrated in Fig. 4, which shows calculation results for the steady-state Taylor deformation

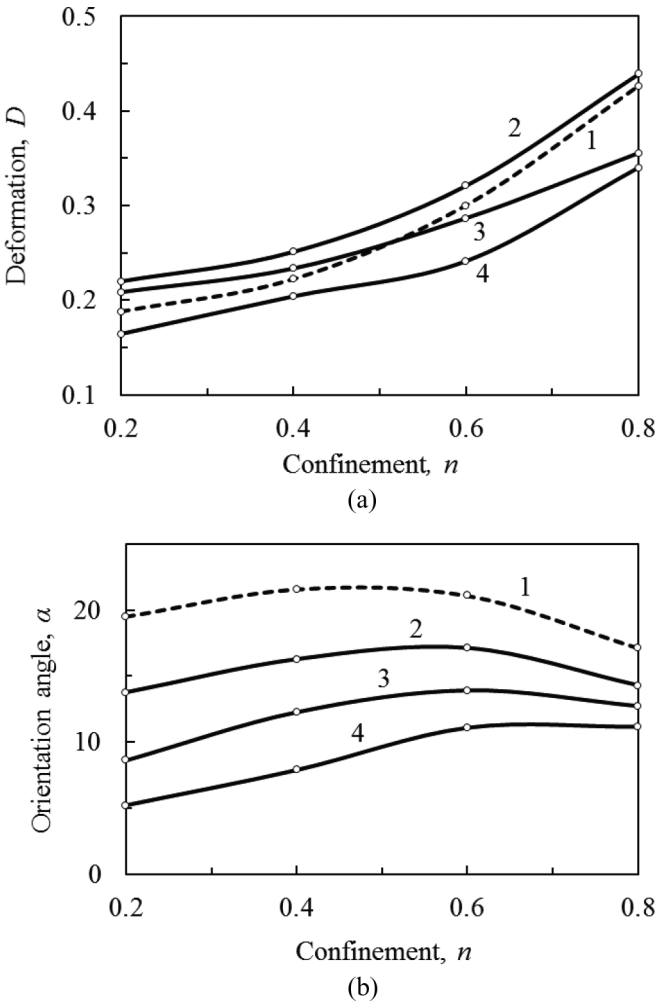

FIG. 4. The dependences of (a) the steady-state Taylor deformation D and (b) orientation angle α of homogeneous and composite droplets on the confinement parameter n at different radii: $k =$ (1) 0 (homogeneous droplet), (2) 0.4, (3) 0.6, and (4) 0.8 at $\mathrm{Ca} = 0.2$, $\mathrm{Re} = 0.05$, $m_{21} = m_{31} = 1$, $\kappa = 1$.

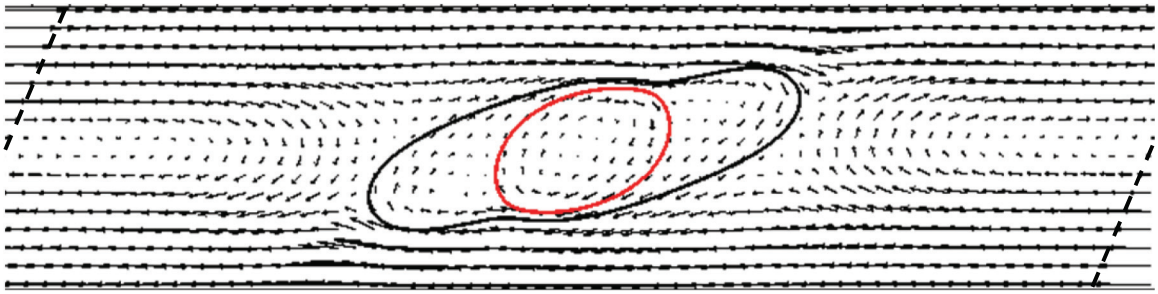

FIG. 5. (Color online) Velocity vector field of the concentric equiviscous composite droplet with the matched interfacial tensions at $k = 0.6$, $n = 0.8$, and $\mathrm{Ca} = 0.4$. The dashed lines indicate velocity profile at the side faces of the computational domain.

D and orientation angle α of the composite droplets versus confinement parameter n at different ratios k of core and shell radii. The calculations were performed for the equiviscous system ($m_{21} = m_{31} = 1$) and matched interfacial tensions on the internal and external droplet boundaries ($\kappa = 1$). The Reynolds and capillary numbers are taken small enough, $\mathrm{Re} = 0.05$ and $\mathrm{Ca} = 0.2$, to neglect inertia and attain droplet stability. It is seen that the Taylor deformation of the composite droplet increases with the increase of the confinement parameter n for all values of k and is not qualitatively different from the behavior of the homogeneous droplet [Fig. 4(a)]. As in the latter case, the additional stretching indicates an increase in the shear stress acting on the outer layer of the droplets on the side of walls [43]. It should be noted that an increase in the core radius results in a decrease in the overall deformation of the composite droplet.

Regarding the orientation angle α of the composite droplet, it passes through the maximum: at small values of confinement parameter n, the orientation angle increases compared with a similar droplet in an unbounded medium while it begins falling at sufficiently large values of n, which is indicative of transition to alignment along the flow direction [see Fig. 4(b)]. The essential difference from the homogeneous droplet is that with increasing core-to-shell radii ratio k, the orientation angle α of the composite droplets decreases and its maximum value is shifted towards larger n. To explain this effect, let us consider the velocity vector field shown in Fig. 5 for the concentric composite droplet with the radii ratio $k = 0.6$ at $n = 0.8$ and $\mathrm{Ca} = 0.4$. Stretching of the droplet leads to an increase in the curvature of the ends and, consequently, an increase of the local Laplace pressure. In turn, this will result in pressure lowering on the left and right of the droplet, thus inducing the upward and downward secondary streams (see Figs. 5 and 8). This entails an increase in the orientation angle.

On the other hand, the narrowing of the channel brings about an increase in the shear rate between the droplet ends and the channel walls, which, in contrast, reduces the orientation angle. It can be concluded that at small n the lateral upward and downward secondary streams dominate, while at large values of the confinement parameter, the near-wall shear flow takes an advantage. Increasing the relative size of the core initiates an increase in the curvature of the tips of the shearing composite droplet. Therefore, its alignment occurs at larger confinement. This explains the shift of the maximum orientation angle towards higher values of n. The decrease in orientation angle of the composite droplet with core-to-shell radii ratio k is associated with the increase in shear rate in the shell, which in turn leads to an increase in the shear rate between the droplet and the channel walls.

It should be noted that in the considered case the velocity profiles near the side faces of the computational domain are practically coincide with the basic linear velocity profile of

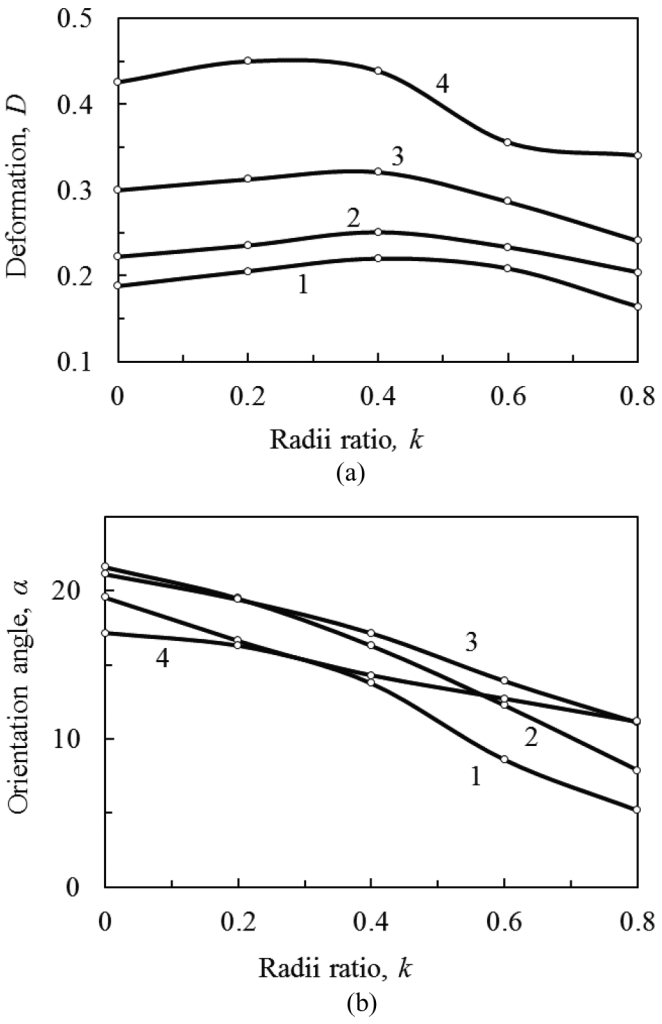

FIG. 6. The dependences of (a) the steady-state Taylor deformation D and (b) orientation angle α of the composite droplet on radii ratio k at different confinement parameters $n =$ (1) 0.2 (2) 0.4 (3) 0.6, and (4) 0.8 at $\mathrm{Ca} = 0.2$, $\mathrm{Re} = 0.05$, $m_{21} = m_{31} = 1$, $\kappa = 1$.

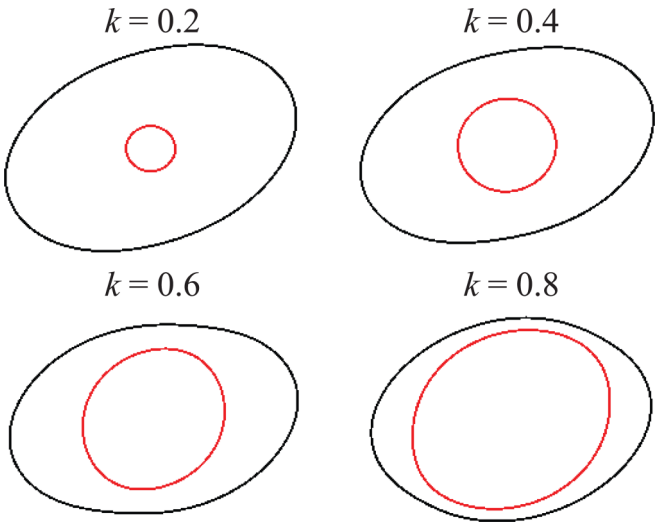

FIG. 7. (Color online) Steady-state shapes of 2D composite droplets for different values of radii ratio k at $n = 0.4$, Ca = 0.2, Re = 0.05, $m_{21} = m_{31} = 1$, $\kappa = 1$.

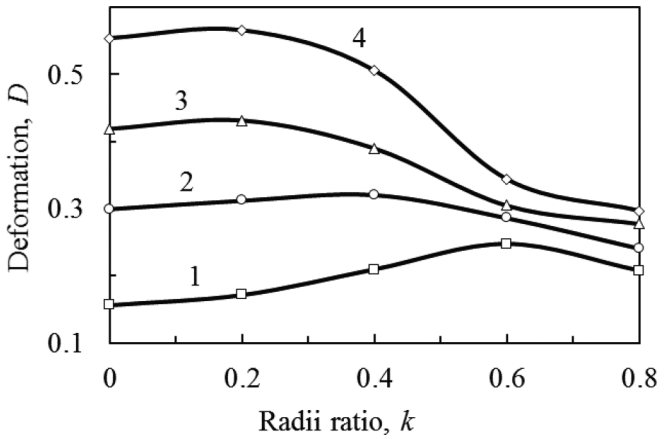

FIG. 9. The steady-state Taylor deformation of the composite droplet vs radii ratio k at $n = 0.6$ for different capillary numbers: Ca = (1) 0.1, (2) 0.2, (3) 0.3, (4) 0.4.

the unperturbed continuous phase. In Fig. 5 this fact is demonstrated by the dashed slanting lines. This clearly indicates that interactions of the front of the droplet with the flow after its back part, caused by the periodic boundary conditions, can be neglected. In the case of smaller values of Ca and n the influence of the side faces of the computational domain is even less. This means that the revealed hydrodynamic effects are inherent to a single composite droplet.

B. The effect of core-to-shell radii ratio

Figure 6 presents dependences of the steady-state Taylor deformation and orientation angle of composite droplets on radii ratio k at different values of the confinement parameter. As in the previous part, the calculations were conducted for the components with equal viscosities and interfacial tensions; the Reynolds and capillary numbers are assigned as Ca = 0.2 и Re = 0.05. It is seen that deformation curves pass through the maxima at all values of the confinement parameter. The nonmonotonous behavior is explained by the so-called "sustaining" effect [28] when the external interface of the composite drop is located in close proximity to the internal interface. In this case, the core begins to interfere with the deformation of the shell.

This effect is illustrated in Fig. 7, which presents the computed steady-state shapes of composite droplets at different core-to-shell radii ratios k for the fixed confinement parameter $n = 0.4$. We can see that when $k > 0.5$ the core prevents stretching of the shell [Fig. 6(a), curve 3]. In contrast, at smaller k the core contributes to the elongation of the composite droplet. The origin of this phenomenon can be revealed by a comparison of pressure fields developed in the homogeneous and composite droplets during shear flow, which is shown in Fig. 8. It is evident that shear flow initiates a depression in the middle part of the shell of the composite droplet [Fig. 8(b)] as compared with a similar homogeneous droplet. This facilitates the compression of the external interface towards the core, which ultimately leads to an increase in the overall elongation of the composite droplet. At the same time, the orientation angle of the composite droplet decreases with increasing core-to-shell radii ratio for all values of the confinement parameter n [Fig. 6(a)]. In other words, the presence of the core promotes a decrease of the orientation angle of the composite droplet.

Figure 9 shows that an increase in capillary number leads to a shift of maximal deformations towards the lower core-to-shell radii ratios. The reason is that, at higher capillary

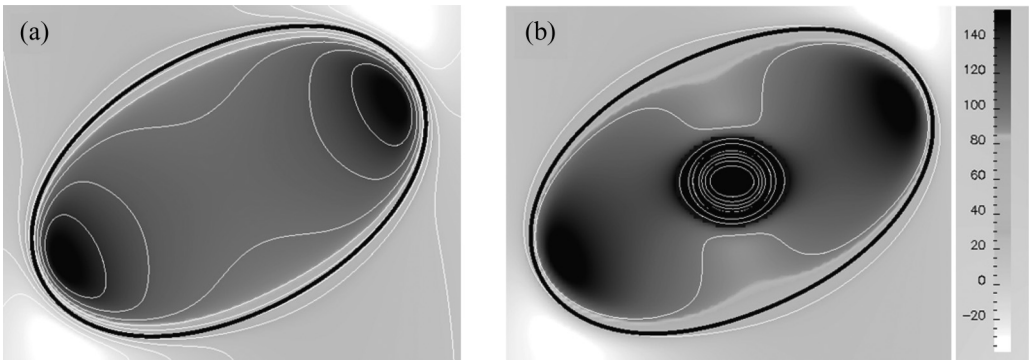

FIG. 8. The pressure fields in (a) homogeneous and (b) composite droplets at $k = 0.2$, $n = 0.6$, Ca = 0.2, Re = 0.05, $m_{21} = m_{31} = 1$, $\kappa = 1$. White lines represent equipressure levels. The scale corresponds to gradation of pressure.

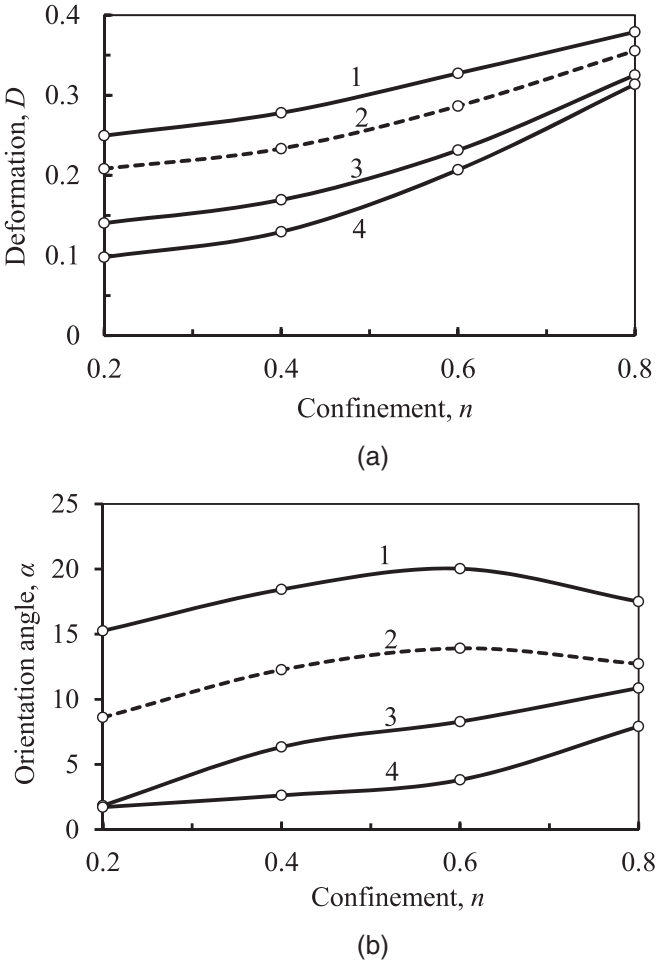

FIG. 10. (a) The steady-state Taylor deformation D and (b) orientation angle α of the composite droplet vs confinement parameter n for different viscosity ratios $m_{21} = (1)\ 0.1$, (2) 1, (3) 3, and (4) 5 at Ca $= 0.2$, Re $= 0.05$, $k = 0.6$, and $\kappa = 1$.

numbers, the composite droplet is stretched more and the "sustaining" effect comes into play at smaller core sizes.

C. The effect of material characteristics

So far we have restricted our consideration to equiviscous fluids with equal interfacial tensions between the conjugated phases. Let us analyze the influence of variations of viscosities and interfacial tensions of the system components. As is known, the relative viscosity of the core has little effect on the deformation behavior of the unbounded composite droplets for both axisymmetric and shear flows [2,29]. Thus, here we will discuss only variations in the relative viscosity of the shell with equiviscous core and continuous phase at different values of confinement parameter n. Figure 10(a) shows dependences of the steady-state Taylor parameter D on n for different viscosity ratios m_{21} calculated at Ca $= 0.2$, Re $= 0.05$, radii ratio $k = 0.6$, and matched interfacial tensions. It can be seen that the increase in the confinement parameter results in an increase of D at all m_{21} values. However, the increase in the relative viscosity of the shell involves a decrease in the overall deformation of composite droplets.

Figure 10(b) shows the influence of the relative viscosity m_{21} of the shell on the orientation angle α of such drops. It can be seen that when the viscosity of the outer layer 2 of the composite droplet is lower than the viscosity of the continuous phase 1 ($m_{21} < 1$), the orientation angle passes through the maximum with increasing confinement parameter n, as is the case for the system with the equiviscous components (cf. Fig. 4).

However, if the viscosity of the shell exceeds the viscosity of the dispersion fluid ($m_{21} > 1$), then the behavior of α with n changes qualitatively: the orientation angle of the composite drop varies monotonically over the entire confinement parameter range. This is due to the relative decrease in the shear rate over the more viscous shell and, as a result, the

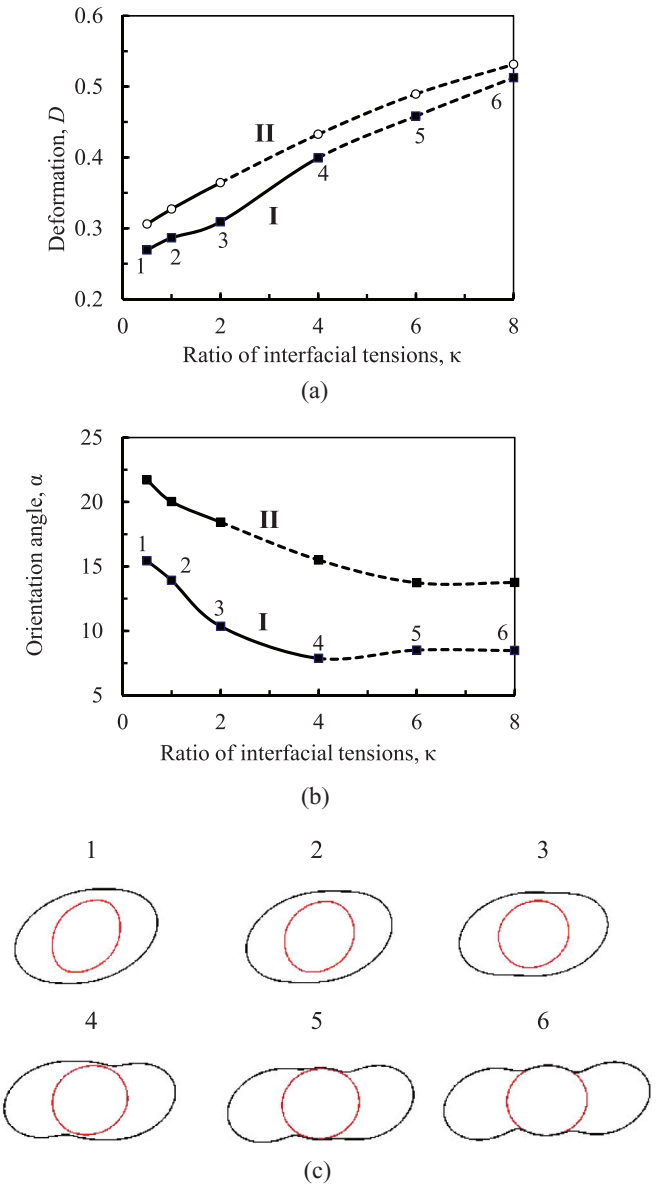

FIG. 11. (Color online) (a) The steady-state Taylor deformation D and (b) orientation angle α of the composite droplet vs interfacial tension ratio κ for viscosity ratios m_{21} equal to (I) 1 and (II) 0.1; (c) the steady-state shapes of composite droplets corresponding to the numbered points.

domination of the downstream and upstream secondary flows on the left and right of the droplet controlling the increase in the orientation angle with n.

Figure 11 represents dependences of the steady-state Taylor deformation D and orientation angle α on the ratio $\kappa = \sigma_{23}/\sigma_{12}$ of interfacial tensions on the inner and external interfaces of the composite droplet. The calculations were performed for two values of viscosity ratio $m_{21} = 1$ (curve I) and $m_{21} = 0.1$ (curve II) at the fixed geometrical $n = 0.6$, $k = 0.6$ and flow parameters, $\mathrm{Ca} = 0.2$ и $\mathrm{Re} = 0.05$. It can be seen that the increase in κ is accompanied by increasing deformation [Fig. 11(a)], while the orientation angle decreases [Fig. 11(b)]. In this case, each κ value corresponds to the certain steady-state composite droplet shape represented in Fig. 11(c) for $m_{21} = 1$. It follows that at $\kappa \geqslant 4$ the external interface almost touches the core of the droplet. This sustaining leads to transformation of the residual portion of the shell into symmetrical earlike projections. These forms of the composite droplets correspond to the dashed parts of deformation curves I in Figs. 11(a) and 11(b). At the same time, in the composite droplet with less viscous shell the sustaining effect comes into play at a smaller ratio of interfacial tensions, $\kappa \sim 2$ (curves II). This is due to the fact that an increase in the core-shell interfacial tension results in the formation of a depression zone in the mid part of the viscous shell. Consequently, the external interface approaches the core, which, in turn, leads to a displacement of shell fluid to the side projections that are more pronounced in a less viscous shell.

Note that the level set function method used in this work to reconstruct the current position of the interfaces is not adapted to simulate the break-up of the interface of the outer layer, which may bring an internal core into direct contact with the dispersion fluid. For this reason, forms 5 and 6 of the composite droplets presented in Fig. 11 should not be considered as final solutions. In the case of rupture of the thin external layer, the observed protrusions may transform into another form depending on the mutual wetting of the three components.

IV. CONCLUSION

The hydrodynamic behavior of a composite droplet in a narrow channel under simple shear flow was investigated by means of numerical simulations. It is shown that an increase in confinement parameter due to the channel narrowing or magnification of drop size results in growth of the steady-state deformation of the composite droplets as was observed before in the case of homogeneous droplets [38,43,44]. This effect takes place at arbitrary ratios of core-to-shell radii, viscosities, interfacial tensions, and capillary numbers. Nonmonotonic behavior of the steady-state Taylor deformation as a function of the radii ratio was found. This is explained by the "sustaining" effect from the core. The increase in the confinement results in a shift of the maximum deformation towards a smaller core-to-shell radii ratio. A similar effect takes place with an increase of the capillary number. The growth of the shell's relative viscosity is always accompanied by a reduction of the overall droplet deformation at any confinement parameter. In contrast, when increasing the relative core-shell interfacial tension, the steady-state deformation increases as well.

Channel narrowing entails a nonmonotonic variation in the steady-state orientation angle of a composite droplet. This angle reduces with increasing core-to-shell radii ratio while its maximum shifts towards larger values of the confinement parameter. This is due to the competition between the near-wall shear flow and downward and upward secondary streams caused by the pressure drop in the vicinity of the droplet tips. The orientation angle of the composite droplet decreases with the increase in the shell's relative viscosity and/or core-shell interfacial tension.

ACKNOWLEDGMENT

This work was supported by the Russian Foundation for Basic Research (Russian Federation), Project No. 13–03–00725.

[1] J. M. Rallison, Annu. Rev. Fluid Mech. **16**, 45 (1984).
[2] H. A. Stone, Annu. Rev. Fluid. Mech. **26**, 65 (1994).
[3] J. M. Ottino, P. DeRoussel, S. Hansen, and D. V. Khakhar, Adv. Chem. Eng. **25**, 105 (1999).
[4] C. L. Tucker III and P. Moldenaers, Annu. Rev. Fluid. Mech. **34**, 177 (2002).
[5] H. F. Guo, S. Packirisamy, N. V. Gvozdic, and D. J. Meier, Polymer **38**, 785 (1997).
[6] J. Reignier and B. D. Favis, Polymer **44**, 5061 (2003).
[7] S. Shokoohi and A. Arefazar, Polym. Adv. Technol. **20**, 433 (2009).
[8] M. A. Letuchii and Y. P. Miroshnikov, J. Macromol. Sci., Part B: Physics **52**, 530 (2013).
[9] S. Torza and S. G. Mason, J. Colloid Interface Sci. **33**, 67 (1970).
[10] J. J. Ulbrecht, P. Stroeve, and P. Prabodh, Rheol. Acta **21**, 593 (1982).
[11] D. Lee and D. A. Weitz, Adv. Mater. **20**, 3498 (2008).
[12] G. Coupier, B. Kaoui, T. Podgorski, and C. Misbah, Phys. Fluids **20**, 111702 (2008).
[13] G. Danker, P. M. Vlahovska, and C. Misbah, Phys. Rev. Lett. **102**, 148102 (2009).
[14] T. Krüger, B. Kaoui, and J. Harting, J. Fluid. Mech. **751**, 725 (2014).
[15] B. F. Gibbs, S. Kermasha, I. Alli, and C. N. Mulligan, Int. J. Food. Sci. Nutr. **50**, 213 (1999).
[16] A. Madene, M. Jacquot, J. Scher, and S. Desobry, Int. J. Food. Sci. Technol. **41**, 1 (2006).
[17] R. Langer, Nature (London) **392**, 5 (1998).
[18] E. Rushton and G. A. Davies, Int. J. Multiphase Flow **9**, 337 (1983).
[19] R. E. Johnson and S. S. Sadhal, J. Fluid. Mech. **132**, 295 (1983).
[20] R. E. Johnson and S. S. Sadhals, Ann. Rev. Fluid Mech. **17**, 289 (1985).
[21] S. S. Sadhal and H. N. Oguz, J. Fluid. Mech. **160**, 511 (1985).
[22] R. M. Rasmussern, V. Levizzanvi, and H. R. Pruppachehr, Pure Appl. Qeophys. **120**, 702 (1982).
[23] H. A. Stone and L. G. Leal, J. Fluid Mech. **211**, 123 (1990).
[24] H. C. Kan, H. S. Udaykumar, W. Shyy, and R. Tran-Son-Tay, Phys. Fluids **10**, 760 (1998).

[25] H. Power, Math. Methods Appl. Sci. **16**, 61 (1993).
[26] K. A. Smith, J. M. Ottino, and M. Olvera de la Cruz, Phys. Rev. Lett. **93**, 204501 (2004).
[27] M. Sussman, P. Smereka, and S. Osher, J. Comput. Phys. **114**, 146 (1994).
[28] I. V. Kravchenko and S. A. Patlazhan, Doklady Phys. Chem. **427**, 155 (2009).
[29] Y. Chen, X. Liu, and M. Shi, Appl. Phys. Lett. **102**, 051609 (2013).
[30] S. A. Patlazhan, I. V. Kravchenko, T. V. Budtova, and V. G. Sultanov, Doklady Phys. Chem. Part 1 **454**, 8 (2014).
[31] A. Zanina and T. Budtova, Macromolecules **35**, 1973 (2002).
[32] B. J. Kirby, *Micro- and Nanoscale Fluid Mechanics Transport in Microfluidic Devices* (Cambridge University Press, Cambridge, 2010).
[33] P. Tabeling, *Introduction to Microfluidics* (Oxford University Press, Oxford, New York, 2010).
[34] R. Seemann, M. Brinkmann, T. Pfohl, and S. Herminghaus, Rep. Prog. Phys. **75**, 016601 (2012).
[35] K. B. Migler, Phys. Rev. Lett. **86**, 1023 (2001).
[36] J. A. Pathak and K. B. Migler, Langmuir **19**, 8667 (2003).
[37] V. Sibillo, G. Pasquariello, M. Simeone, V. Cristini, and S. Guido, Phys. Rev. Lett. **97**, 054502 (2006).
[38] P. J. A. Janssen, A Vananroye, P. Van Puyvelde, P. Moldenaers, and P. D. Anderson, J. Rheol. **54**, 1047 (2010).
[39] M. Shapira and S. Haber, Int. J. Multiphase Flow **16**, 305 (1990).
[40] G. I. Taylor, Proc. R. Soc. London Ser. A **146**, 501 (1934).
[41] M. Minale, Rheol. Acta. **47**, 667 (2008).
[42] P. L. Maffettone and M. Minale, J. Non-Newt. Fluid Mech. **78**, 227 (1998).
[43] Y. Renardy, Rheol. Acta. **46**, 521 (2007).
[44] P. J. A. Janssen and P. D. Anderson, J. Comp. Phys. **227**, 8807 (2008).
[45] S. Farokhirad, T. Lee, and J. F. Morris, Commun. Comput. Phys. **13**, 706 (2013).
[46] G. Tomaiuolo and S. Guido, Microvascular Res. **82**, 35 (2011).
[47] S. M. Hosseini and J. J. Feng, Biophys. J. **103**, 1 (2012).
[48] J. D. Tice, A. D. Lyon, and R. F. Ismagilov, Anal. Chimica Acta **507**, 73 (2004).
[49] V. Srinivasan, V. K. Pamula, and R. B. Fair, Anal. Chimica Acta **507**, 145 (2004).
[50] S. Y. Teh, R. Lin, L. H. Hung, and A. P. Lee, Lab Chip **8**, 198 (2008).
[51] J. S. Sander, L. Isa, P. A. Rühs, P. Fischerc, and A. R. Studart, Soft Matter **8**, 11471 (2012).
[52] J. U. Brackbill, D. B. Kothe, and C. Zemach, J. Comp. Phys. **100**, 335 (1992).
[53] M. Sussman, E. Fatemi, P. Smereka, and S. Osher, Comput. Fluids **27**, 663 (1998).
[54] J. Li, Y. Renardy, and M. Renardy, Phys. Fluids **10**, 3056 (1998).